Modeled reconstructions of the oceanic carbonate system for different histories of atmospheric carbon dioxide during the last 20 Ma

Christopher D. Roberts[1] and Aradhna K. Tripati[1]

Received 17 July 2008; revised 2 December 2008; accepted 26 December 2008; published 11 March 2009.

[1] A box model was used to estimate oceanic carbonate system parameters (total dissolved inorganic carbon, alkalinity, $CO_{2(aq)}$, CO_3^{2-}, HCO_3^-, and pH) in the surface and deep ocean over the past 20 Ma. Geological data were used to constrain boundary conditions, including the carbonate compensation depth (CCD) and seawater temperature, salinity, and ionic composition. In addition, ~14,000 $\delta^{13}C$ measurements of planktic and benthic foraminifera were compiled. Sensitivity tests were performed to evaluate potential errors arising from uncertainties in model boundary conditions. Values of surface water pH were modeled assuming four different histories of atmospheric CO_2, and compared with proxy-based estimates of pH. The system is underconstrained, and therefore multiple CO_2 histories can be invoked to explain the same pH trend, depending on the assumptions made regarding ocean overturning and biological productivity. Despite this uncertainty, we conclude that if CO_2 was strongly coupled to temperature and ice volume over the last 20 Ma, predicted values of surface ocean pH fit poorly with current proxy-based pH reconstructions.

Citation: Roberts, C. D., and A. K. Tripati (2009), Modeled reconstructions of the oceanic carbonate system for different histories of atmospheric carbon dioxide during the last 20 Ma, *Global Biogeochem. Cycles*, *23*, GB1011, doi:10.1029/2008GB003310.

1. Introduction

[2] Ice cores recovered from Antarctica provide us with a direct record of atmospheric CO_2 for the last 800,000 years [*Petit et al.*, 1999; *Siegenthaler et al.*, 2005; *Luthi et al.*, 2008]. Further back in time, constraints on atmospheric CO_2 or the oceanic carbonate system ($CO_{2(aq)}$, HCO_3^-, CO_3^{2-}, pH, alkalinity, and total dissolved inorganic carbon) are limited. These constraints include several proxy and model reconstructions of atmospheric CO_2 [e.g., *Bergman et al.*, 2004; *Berner and Kothavala*, 2001; *Berner et al.*, 1983; *Cerling*, 1991; *Royer et al.*, 2001], $CO_{2(aq)}$ [*Pagani et al.*, 1999; *Pagani et al.*, 2005a; *Pearson and Palmer*, 1999, 2000], and a single record of ocean pH [*Pearson and Palmer*, 2000].

[3] All of these reconstructions disagree over both the timing and magnitude of large-amplitude (>100 μatm) changes in CO_2 and are low in temporal resolution. Prior to 800,000 years ago, existing reconstructions of CO_2 do not show a simple covariance with proxy records of temperature and ice volume, in contrast to what might be expected. Some CO_2 reconstructions [*Pagani et al.*, 1999; *Pagani et al.*, 2005a] show relatively stable values for the last 20 Ma, despite evidence for major climatic shifts such as the expansion of continental ice sheets in the mid-Miocene and global warmth during the early Pliocene Warm Interval [*Billups and Schrag*, 2002; *Flower and Kennett*, 1995; *Lear et al.*, 2000; *Zachos et al.*, 2001]. Other reconstructions [e.g., *Bergman et al.*, 2004] indicate declining CO_2 during the last 20 Ma. Some estimates derived from paleosols suggest levels may have reached 1000 μatm several times during the Neogene (see *Royer* [2003, 2006] for compilations of CO_2 data).

[4] Our objective was to test the consistency of different reconstructions of CO_2 and surface ocean pH for the last 20 Ma using a simple box model and geological constraints on the processes that influence the long-term evolution of the carbon cycle. A three-box model was used to reconstruct the oceanic carbonate system in the surface and deep ocean for four assumed histories of CO_2 (Figure 1a). Geological data, including estimates of ocean temperature, ocean composition and the carbonate compensation depth were used to place constraints on model boundary conditions. We calibrated the model using data from the preindustrial Holocene and Last Glacial Maximum (LGM) and performed sensitivity analyses to determine which model parameters were responsible for the majority of uncertainty and variance in our calculations. Each of the four CO_2 histories were evaluated by comparing calculated values of surface ocean pH with published estimates based on the boron isotope ($\delta^{11}B$) composition of foraminiferal calcite [*Pearson and Palmer*, 2000].

2. Carbonate System in Seawater

[5] The equations defining the carbonate system are given in Appendix A. There are only two independent variables in this system, which makes it possible to fully reconstruct the

[1]Department of Earth Sciences, University of Cambridge, Cambridge, UK.

0886-6236/09/2008GB003310$12.00

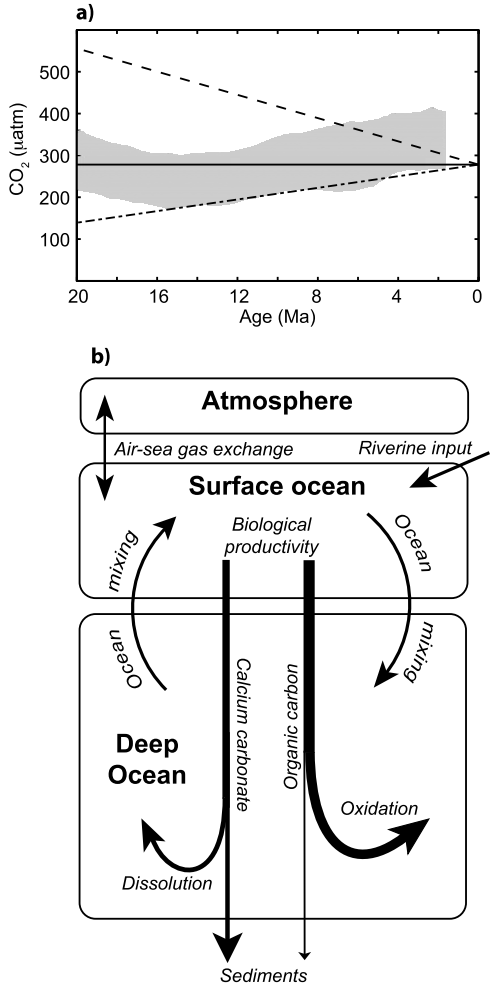

Figure 1. (a) The four records of CO_2 used to reconstruct the oceanic carbonate system for the past 20 Ma. We used three simple linear histories (constant CO_2, solid line; halved CO_2, dashed line; doubled CO_2, dot-dashed line) and a record derived from proxy data (mean values vary between 200 and 300 μatm; shaded area covers values within 95% uncertainty bands). (b) A schematic diagram of the three-box model of the carbon cycle built for this study.

system when values for any two of the six parameters (CO_2, HCO_3^-, CO_3^{2-}, pH, DIC, and alkalinity) are known. For further details of these calculations and a more thorough description of the carbonate system in seawater, refer to *Zeebe and Wolf-Gladrow* [2001].

3. Methods

3.1. Model Description

[6] The three-box model we use (Figure 1b) includes boxes for the atmosphere, surface ocean (depth 0–200 m) and deep ocean (depth > 200 m). Simple models with two ocean reservoirs were first used by Broecker and coworkers in the early 1980s [e.g., *Broecker and Peng*, 1982]. Subsequent studies used more complex four- and five-box models to investigate CO_2 changes over glacial-interglacial time scales [e.g., *Knox and McElroy*, 1984; *Sarmiento and Toggweiler*, 1984; *Siegenthaler and Wenk*, 1984]. Although the three-box model we have used is a very primitive representation of the carbon cycle, we used it to study changes over multimillion year time scales because it gives the greatest transparency with the simplest possible representation of vertical gradients in the ocean.

3.1.1. Air-Sea Exchange

[7] The net flux of CO_2 into the surface ocean ($F_{air\text{-}sea}$) from the atmosphere was parameterized using the following relationship from *Takahashi et al.* [1997]: $F_{air\text{-}sea} = A.E.\Delta CO_2$, where A is the sea surface area, E is the gas transfer coefficient, and ΔCO_2 is the CO_2 concentration gradient between the surface ocean and the atmosphere. E was evaluated for an average wind speed of 7.5 m/s using the relationship formed by *Wanninkhof* [1992]. For our purposes, CO_2 in the atmosphere was kept constant, in order to fix surface ocean values at a specific level of CO_2 and to speed up model equilibration.

3.1.2. Biological Productivity and Ocean Turnover

[8] Biological productivity was parameterized as fluxes of alkalinity and DIC. The ratio of alkalinity/DIC moved from the surface to the deep ocean was controlled by the export flux of organic carbon (P) and the ratio of $CaCO_3$/organic carbon productivity (r). Although we did not explicitly trace nutrients, we did include a correction for alkalinity associated with nitrate that is assimilated into organic material. For every positive flux of organic carbon, we included a negative flux of alkalinity in a 106:16 ratio. An exchange flux of water (F_{mix}) mixed the surface and deep ocean reservoirs to represent ocean-overturning processes such as thermohaline circulation and vertical mixing.

3.1.3. Carbonate Compensation Depth

[9] The depth below which no $CaCO_3$ is preserved in deep ocean sediments is termed the carbonate compensation depth (CCD) [*Broecker and Peng*, 1982]. CCD variations are evidence for changes in the calcite saturation state (Ω) of the deep ocean. Ω describes whether or not calcite is thermodynamically stable in a solution:

$$\Omega = \frac{[Ca^{2+}].[CO_3^{2-}]}{K_{sp}(P, T, solution\ composition)} \quad (1)$$

K_{sp} is the solubility product of calcite and is a function of temperature, pressure, and the ionic composition of the solution. If $\Omega > 1$ then the solution is supersaturated and calcite is stable whereas if $\Omega < 1$ the solution is undersaturated and calcite is unstable. We determined the depth of the calcite saturation horizon in the deep ocean box by calculating the depth at which $\Omega = 1$.

[10] For simplicity in the model, the calcite saturation horizon and the CCD were considered to be at equivalent depths. However, we note that because the dissolution of calcite is kinetically controlled [*Morse and Arvidson*, 2002], $CaCO_3$ accumulation rates are usually sufficient to suppress the CCD to depths below the saturation horizon. In addition, in some oceanic regions the oxidation of organic carbon by bacteria in sediments can cause pore waters to become more

acidic leading to diagenetic (or respiratory) dissolution of calcite within the sediments at depths well above the saturation horizon [*Emerson and Bender*, 1981].

3.1.4. Sedimentary and Weathering Fluxes

[11] The model was run as an open system, with both DIC and alkalinity continuously added to the surface ocean to represent the riverine input of weathering products and removed from the oceans by sedimentary fluxes. The burial flux of $CaCO_3$ in the deep ocean ($CaCO3_{pelagic}$) was calculated at each time step by estimating the area of the ocean floor oversaturated with respect to calcite using the relationship:

$$CaCO3_{pelagic} = MAR_{CaCO3} \times \int_{200m}^{CCD} hypsometry(z).dz \quad (2)$$

where MAR_{CaCO3} was the average mass accumulation rate of $CaCO_3$ in the deep ocean, hypsometry(z) was a polynomial function derived from the hypsometry data of *Menard and Smith* [1966], and z was depth in the ocean. By allowing deep ocean $CaCO_3$ sedimentation to be a function of the CCD, the model incorporated a simple feedback to approximate the process of carbonate compensation. The model can therefore also be used for transient experiments, although no transient results are presented here.

[12] For simulations covering the last 20 Ma, "net weathering" of DIC and alkalinity (the flux that reaches beyond coastal deposition) was adjusted to reproduce the trends in the CCD. Previous studies [e.g., *Kump and Arthur*, 1997; *Kump et al.*, 2000] have noted that the depth of the CCD is probably a poor indicator of global weathering rates and in fact it is more likely to reflect changes in the capacity for $CaCO_3$ deposition in shallow coastal regions.

3.1.5. Estimation of Constants

[13] Calculating CO_2, CO_3^{2-}, HCO_3^-, and pH from DIC and alkalinity values requires estimates for the carbonic acid dissociation constants (k_1 and k_2), the solubility of CO_2 in seawater (k_{CO2}), the ionic product of water (k_w) and the dissociation constant of boric acid (k_B). Evaluation of Ω also requires the estimation of the solubility product of calcite (K_{sp}).

[14] We calculated all constants as a function of solution composition, as well as temperature and pressure (see Appendix B for the method used). For elements other than Mg^{2+} and Ca^{2+}, estimates of salinity were used to scale concentrations relative to modern values. We used the reconstructed history of seawater Mg^{2+} and Ca^{2+} compiled by *Tyrrell and Zeebe* [2004]. However, we note that given the uncertainty in proxy data [*Dickson*, 2002; *Horita et al.*, 2002; *Lowenstein et al.*, 2001; *Wilkinson and Algeo*, 1989; *Zimmermann*, 2000], seawater Mg^{2+} and Ca^{2+} concentrations are not well constrained.

3.2. Model Solutions

[15] All fluxes within the model were described in terms of DIC and alkalinity because these are the two parameters within the carbonate system whose values are unaffected by pH, temperature or salinity. The ordinary differential equations used to describe the evolution of DIC, alkalinity and $\delta^{13}C$ in each model reservoir are as follows:

$$\frac{dM_{CO2}}{dt} = -F_{air-sea}$$

$$M_s.\frac{dDIC_s}{dt} = F_{DIC} + F_{air-sea} + F_{mix}.(DIC_d - DIC_s) - P.(1+r) - CaCO_{3shelf} - Corg_{shelf}$$

$$M_d.\frac{dDIC_d}{dt} = F_{mix}.(DIC_s - DIC_d) + P.(1+r) - CaCO_{3pelagic} - Corg_{pelagic}$$

$$M_s.\frac{dALK_s}{dt} = F_{ALK} - F_{NO3} + F_{mix}.(ALK_d - ALK_s) - 2.P.r - 2.CaCO_{3shelf} + \frac{16}{106}.\left(P + Corg_{shelf}\right)$$

$$M_d.\frac{dALK_d}{dt} = F_{mix}.(ALK_s - ALK_d) + 2.P.r - 2.CaCO_{3pelagic} + \frac{16}{106}.\left(Corg_{pelagic} - P\right)$$

$$M_s.DIC_s.\frac{d\delta^{13}C_s}{dt} = F_{DIC}.\left(\delta^{13}C_{riv} - \delta^{13}C_s\right) + F_{mix}.DIC_d.\left(\delta^{13}C_d - \delta^{13}C_s\right) - \Delta Corg.\left(P + Corg_{shelf}\right)$$

$$M_d.DIC_d.\frac{d\delta^{13}C_d}{dt} = \left(F_{mix}.DIC_s + P.r - CaCO_{3pelagic}\right).\left(\delta^{13}C_s - \delta^{13}C_d\right) + \left(P - Corg_{pelagic}\right).\left(\delta^{13}C_s + \Delta Corg - \delta^{13}C_d\right)$$

These equations were solved at 1 Ma intervals since 20 Ma using Matlab and Simulink (c) such that each time slice represented a steady state solution from a transient simulation lasting ~1 Ma.

3.3. Model Boundary Conditions

[16] Model boundary conditions were constrained using proxy and geological data. Figure 2 shows the records used for Mg^{2+} and Ca^{2+} concentrations, ocean salinity, surface and deep ocean temperature, CCD, and the photosynthetic fractionation of carbon. Late Holocene values were used to define model boundary conditions without available geological constraints (e.g., the $CaCO_3/C_{org}$ export ratio).

3.3.1. Atmospheric CO_2

[17] We forced the model with four different records of CO_2 (Figure 1a), three of which (constant, doubled, and halved CO_2) were simplified linear trends between 20 and 0 Ma. The remaining CO_2 history was derived predominantly from the $\delta^{13}C$-alkenone based record for 20–5 Ma [*Pagani et al.*, 2005a] and supplemented with stomatal density data from fossilized leaves for 5–2 Ma [*Kurschner et al.*, 1996] because of the lack of published $\delta^{13}C$-alkenone data for 5–2 Ma. The records used as model constraints were smoothed 95% confidence bands (statistical methods are described in Appendix C) generated from the proxy data.

3.3.2. Biological Productivity, Ocean Turnover, and Surface to Deep $\delta^{13}C$ Gradients

[18] The "biological pump" transfers isotopically light organic carbon from the surface to the deep ocean. Ocean

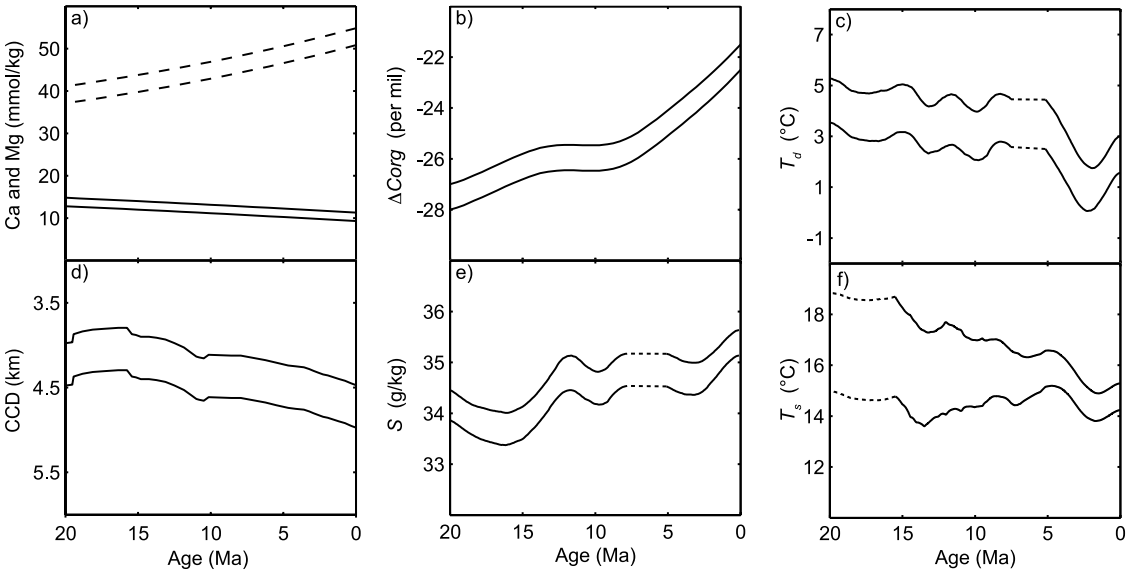

Figure 2. Boundary conditions from the geological record used as model constraints for the last 20 Ma. (a) Records of Ca^{2+} (solid lines) and Mg^{2+} (dashed lines) from *Tyrrell and Zeebe* [2004] based on the "best guess estimates" of *Horita et al.* [2002]. Estimated uncertainty of ±1 mmol/kg for Ca^{2+} and ±2 mmol/kg for Mg^{2+}. (b) Photosynthetic fractionation of carbon estimated from paired $\delta^{13}C$ measurements of organic carbon and calcite [*Hayes et al.*, 1999]. Uncertainty of ±0.5‰ was chosen to fit the reported error of ±1 s.d. (c) Smoothed 95% confidence curves for deep ocean temperature estimated using Mg/Ca data from benthic foraminifera [*Billups and Schrag*, 2002]. Uncertainties were interpolated between 5.0 and 7.5 Ma because of low data density. (d) Globally averaged record of CCD from *Sime et al.* [2007], based on data from *Lyle* [2003] and *Thunell and Corliss* [1986]. Estimated uncertainty ±250 m. (e) Smoothed 95% confidence bands for salinity estimated using $\delta^{18}O_{sw}$ data from benthic foraminifera [*Billups and Schrag*, 2002]. Uncertainties were interpolated between 5.0 and 7.5 Ma because of poor data density. $\delta^{18}O_{sw}$ was translated into salinity assuming a 1‰ shift for every 100 m of sea level change. (f) Average surface ocean temperature. Tropical sea surface temperature ($T_{tropical}$) estimated using records of Mg/Ca from planktic foraminifera [*Sime*, 2006; *Wara et al.*, 2005; S. A. Nathan and R. M. Leckie, unpublished data, 2008]. Confidence bands were extrapolated from 16 to 20 Ma because of poor data density. Average surface ocean temperature (T_s) was then estimated using the relationship $T_s = (T_{tropical} + T_d)/2$ where it was assumed that deep ocean temperatures (T_d) from Figure 2c were representative of surface ocean temperatures in the high latitudes.

mixing processes (designated F_{mix} in the model) act to homogenize the ocean and reduce the $\delta^{13}C$ gradient between the surface and deep ocean ($\Delta\delta^{13}C$). It was not possible to directly constrain either ocean mixing (F_{mix}) or biological productivity (P) using published data for the studied interval. However, large changes to either F_{mix} or P should influence $\Delta\delta^{13}C$.

[19] We made two assumptions regarding vertical geochemical gradients in the ocean for every model simulation. One set of simulations assumed that biological productivity and ocean turnover were constant for the last 20 Ma. For the second set, we used $\delta^{13}C$ data as a model boundary condition to set P and F_{mix}. The model was tuned to a specific value of $\Delta\delta^{13}C$ by keeping P constant and changing the magnitude of F_{mix}.

3.3.3. A 20 Ma Composite Record of $\delta^{13}C$ in the Surface and Deep Ocean

[20] In order to estimate $\Delta\delta^{13}C$, over 14,000 $\delta^{13}C$ measurements of planktic and benthic foraminifera from the Pacific Ocean were compiled from published records (Figure 3a and Table 1). Oxygen isotope data were also compiled. The full data set includes several records from the previously published benthic isotope stack of *Zachos et al.* [2001]. The compiled isotopic data are available online as auxiliary material.[1]

[21] Planktic $\delta^{13}C$ data were restricted to sites from the low-latitude Pacific (30°N to 30°S) and benthic $\delta^{13}C$ data were restricted to Pacific sites deeper than 1.5 km. Species were limited to *Cibicidoides sp.* and *Uvigerina sp.* for the benthic compilation and *G. ruber*, *G. sacculifer*, and *G. quadrilobatus* for the planktic compilation. All age models were updated to the most recent geomagnetic polarity time scale of *Gradstein et al.* [2004] and $\delta^{13}C$ measurements were corrected to DIC values to account for interspecies offsets following *Shackleton et al.* [1995] and *Spero et al.* [2003]. The final surface and deep ocean records were then smoothed to extract the long-term trends, and 95% confidence bands were calculated.

[1] Auxiliary materials are available at ftp://ftp.agu.org/apend/gb/2008gb003310.

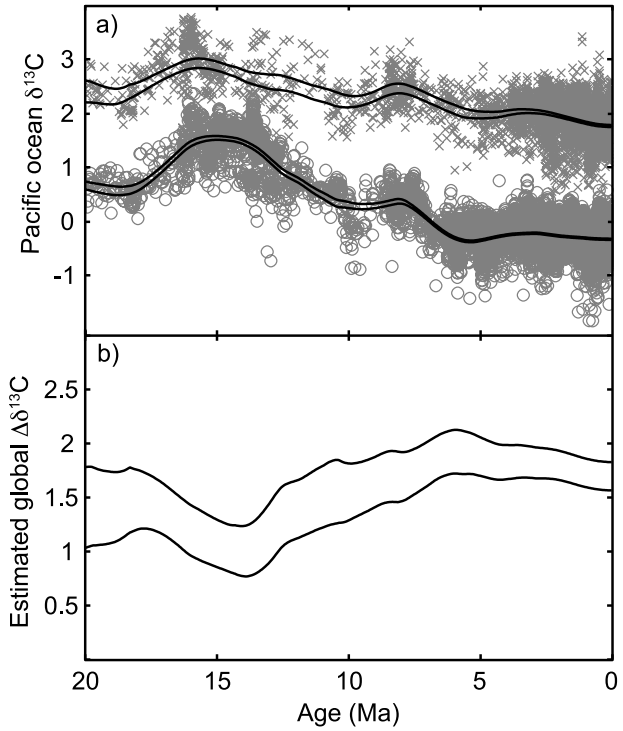

Figure 3. (a) Pacific ocean $\delta^{13}C$ data from planktic (gray crosses) and benthic (gray circles) foraminifera corrected to DIC values of $\delta^{13}C$ following *Spero et al.* [2003] and *Shackleton et al.* [1995] and adjusted to a common age model [*Gradstein et al.*, 2004]. The solid black lines are smoothed 95% confidence bands. (b) Estimated global $\Delta\delta^{13}C$ gradient between the surface and deep ocean. See text for the assumptions we made when constructing this record.

[22] The data for these composite records were sourced from a region of higher than normal productivity, and older than average deep waters. We would therefore expect global average values for $\Delta\delta^{13}C$ to be lower than those estimated from the Pacific data. In order to compare $\Delta\delta^{13}C$ values estimated from data with values calculated with the model, we scaled the Pacific data using the following relationship:

$$\Delta\delta^{13}C_{global(t)} = \Delta\delta^{13}C_{pacific(t)} \times \left(\frac{\Delta\delta^{13}C_{global(0)}}{\Delta\delta^{13}C_{pacific(0)}}\right) \quad (3)$$

where $\Delta\delta^{13}C_{global(t)}$ was the estimated global gradient in the past (Figure 3b), $\Delta\delta^{13}C_{global(0)}$ was the estimated global gradient for the Holocene, $\Delta\delta^{13}C_{pacific(0)}$ was the Pacific gradient at 0 Ma and $\Delta\delta^{13}C_{pacific(t)}$ was the Pacific gradient in the past. Uncertainty in $\Delta\delta^{13}C_{global(t)}$ was estimated to be ±(half the 95% confidence range in planktics + half the 95% confidence range in benthics + 0.1)‰ where the 0.1‰ accounts for the uncertainty in the transformation to global values.

4. Results

4.1. Preindustrial Holocene

[23] Table 2 lists the model values used for the preindustrial Holocene (12–0 ka). Atmospheric CO_2 was set to a preindustrial value of 278 μatm and global average temperatures were assumed to be 15°C for the surface ocean and 4°C for the deep ocean. Salinity, Mg^{2+} and Ca^{2+} concentrations were estimated by scaling values from a standard seawater composition [*Millero*, 2006] to an average ocean salinity of 34.7 g/kg. Riverine and sedimentary fluxes of $CaCO_3$ and organic carbon were chosen to be consistent with modern estimates [e.g., *Collier and Edmond*, 1984; *Delaney and Boyle*, 1988; *Edmond et al.*, 1979; *Kump and Arthur*, 1997; *Lasaga et al.*, 1985] and also such that inputs and outputs from the model system were in balance. P and r were both chosen to fit previous model and data based estimates [*Boyd and Trull*, 2007; *Jin et al.*, 2006, and references therein]. The isotopic fractionation of organic carbon ($\Delta Corg$) was estimated from paired $\delta^{13}C$ measurements of organic carbon and $CaCO_3$ [*Hayes et al.*, 1999; *Kump and Arthur*, 1997]. MAR_{CaCO3} was tuned until the model CCD matched a global average value of 4.75 km [*Broecker and Peng*, 1982] and F_{mix} was adjusted until calculated values for DIC and alkalinity were consistent with oceanographic data from the Geochemical Ocean Sections Study [*Bainbridge*, 1981; *Craig et al.*, 1981; *Spencer et al.*, 1982].

[24] Results for the Holocene (Table 3) were compared to modern data and results from GENIE-1 (used without the terrestrial biosphere module, ENTS), a more complex model of the carbon cycle. For a description of the GENIE-1 model see *Lenton et al.* [2006] and *Ridgwell et al.* [2007]. There was some mismatch between calculated and measured estimates of surface ocean pH and $\Delta\delta^{13}C$. However, this discrepancy occurs because modern measurements of surface ocean pH and $\delta^{13}C$ are not representative of preindustrial values. The addition of very isotopically light carbon from fossil fuels to the atmosphere has led to a decrease in surface ocean $\delta^{13}C$ of ~0.5‰ [*Kroopnick*, 1985] and a decrease in surface ocean pH from 8.2 to 8.1 [*Caldeira and Wickett*, 2003]. If these anthropogenic effects of fossil fuel derived CO_2 on surface ocean $\delta^{13}C$ and pH are taken into account, our model-calculated values for the Holocene are consistent with measurements and the results from GENIE-1.

4.2. Last Glacial Maximum

[25] For the LGM configuration, we used surface and deep ocean temperatures of 11°C and 0°C, CO_2 values of

Table 1. Data Sources Used for the Records of Surface and Deep Ocean $\delta^{13}C$

DSDP/ODP Sites	Reference
77	*Keigwin and Keller* [1984]
206	*Flower and Kennett* [1995]
289	*Gasperi and Kennett* [1993]
586	*Whitman and Berger* [1993]
588	*Miller and Fairbanks* [1985]
588	*Pagani et al.* [1999]
591	*Flower and Kennett* [1995]
806	*Billups et al.* [1999]
846	*Shackleton et al.* [1995]
849	*Mix et al.* [1995]
871	*Pearson and Shackleton* [1995]
1143	*Cheng et al.* [2004a]
1146	*Clemens and Prell* [2003]
1147	*Cheng et al.* [2004b]
1148	*Cheng et al.* [2004b]

Table 2. Holocene Model Configuration

Model Variables	Holocene Values
$\Delta Corg$	−22 per mil
CO_2	278 μatm
F_{ALK}	3.2×10^{13} eq/a
F_{DIC}	2.2×10^{13} mol/a
F_{mix}	4.1×10^{18} kg/a
MAR_{CaCO3}	0.66 g/cm^2/ka
P	7.1×10^{14} molCorg/a
r	0.175
S	34.7 g/kg
$CaCO_{3pelagic}$	1.5×10^{13} mol/a
$CaCO_{3shelf}$	1.0×10^{12} mol/a
$Corg_{pelagic}$	3.0×10^{12} mol/a
$Corg_{shelf}$	3.0×10^{12} mol/a
T_s	4°C
T_d	15°C

185–195 μatm and a salinity of 35.9 g/kg. We estimated the CCD to be between 0 and 500 m deeper than in the Holocene and assumed $\Delta\delta^{13}$C to be between 1.45 and 1.95. All other model parameters were assumed to be the same as those used for the Holocene. Our calculated values for LGM surface ocean pH (8.26–8.32) compared well to both δ^{11}B (8.30–8.34) and B/Ca (8.23–8.32) based proxy estimates [*Hönisch and Hemming*, 2005; *Yu et al.*, 2007]. This comparison demonstrates that the model may be applied to intervals further back in time with some degree of confidence.

4.3. Model Sensitivity Tests

[26] Two sensitivity analyses were performed (Table 4) to identify the model parameters that were responsible for the majority of variance and uncertainty in our results. The first analysis was performed by changing each model variable in isolation and recording the absolute and percentage difference between the calculated outputs and those for the Holocene steady state. For the second analysis we adjusted each model parameter and then tuned F_{mix} until $\Delta\delta^{13}$C reached Holocene values. This second suite of simulations allowed us to characterize the model response to the tuning process.

[27] Both sensitivity analyses showed that the majority of variance and uncertainty for calculations over the last 20 Ma (Table 4) was sourced from (1) changing CO_2, (2) the $\Delta\delta^{13}$C gradient (i.e., the target for tuning F_{mix} and P), (3) Ca^{2+} concentration, and (4) surface ocean temperature. The results also demonstrated that the tuning process exaggerated uncertainty for all variables except P (which showed a near perfect trade-off with F_{mix} when tuning to $\Delta\delta^{13}$C.) Further sensitivity analyses (not presented here) showed that the model responded in a nonlinear fashion for changes to CO_2, Ca^{2+}, and $\Delta\delta^{13}$C. For this reason, the percentage uncertainties in Table 4 are not additive and cannot be directly applied to other model configurations.

[28] Three different parameters were adjusted to test the sensitivity of the model to a ±250 m change in the CCD: the pelagic $CaCO_3$ mass accumulation rate (MAR_{CaCO3}), carbonate shelf sedimentation ($CaCO_{3shelf}$), and continental weathering rates (F_{DIC} and F_{ALK}). These analyses demonstrated that all three parameters exert a strong control on the CCD and that the model is sensitive to these changes. However, the model response to a 250 m shift is within 0.1% for each mechanism used to effect the CCD change.

[29] Changes to the weathering and precipitation rates of large evaporite deposits were not considered when calculating ocean salinity. However, results from sensitivity testing (Table 4) indicated that the model was much less sensitive to the total salinity of the ocean than it was to the ionic composition of the solution. Although SO_4^{2-} concentration was not used as a separate constraint despite a reconstruction being available for the last 10 Ma [*Turchyn and Schrag*, 2004], we did include it as a variable in the sensitivity analyses. The impact of changing SO_4^{2-} by 5 mmol/kg is to change our main results by less than ±0.5%.

[30] Figure 4 compares two methods for estimating K_{sp} as a function of Mg^{2+} and Ca^{2+} (see Appendix B). The values calculated using a simple empirical relationship (Figure 4a) are contradictory to those calculated using a Pitzer equilibrium model (Figure 4b). This finding is because the empirical relationship assumes that K_{sp} is invariant for a given ratio of Mg^{2+}/Ca^{2+}, while in the Pitzer model, Mg^{2+} and Ca^{2+} are independent variables.

4.4. Last 20 Ma

[31] Calculated records for surface and deep ocean alkalinity and DIC, surface ocean pH, and surface ocean CO_3^{2-} for all four histories of CO_2 are displayed in Figures 5–8. Results for deep ocean CO_3^{2-} and the modeled changes in "net weathering" consistent with the record of CCD are shown in Figure 9. For each 20 Ma record and for every time slice, four different model configurations were used in order to propagate the uncertainty present in the geological boundary conditions. The sensitivity tests described in section 4.3 showed that nearly 100% of the variance for alkalinity, DIC, CO_3^{2-} and surface ocean pH could be attained using just four different configurations.

4.4.1. DIC and Alkalinity

[32] For DIC and alkalinity, surface ocean trends mirror those in the deep ocean.

Table 3. Model Results for the Holocene Compared With Modern Data and Also With Results From a 3-D Earth System Model[a]

Variable	This Model	Modern Values	GENIE-1 (<30° Latitude)	GENIE-1 (>30° Latitude)
DIC_s (μmol/kg)	2034	2000–2050[b]	1947	2039
DIC_d (μmol/kg)	2233	2200–2250[b]	2258	2218
ALK_s (μeq/kg)	2333	2300–2350[b]	2297	2301
ALK_d (μeq/kg)	2354	2350–2400[b]	2384	2359
$CO3_s$ (μmol/kg)	206	200–250[b]	246	184
$CO3_d$ (μmol/kg)	93	70–110[b]	94	102
pH_s	8.18	8.1[c]	8.18	8.13
pH_d	7.93	7.7–8.0[c]	7.92	7.96
$\Delta\delta^{13}C$ (per mil)	1.70	1.0–1.5[b]	1.71	1.07

[a]The data from the 3-D Earth System Model (GENIE-1) were separated by latitude and then averaged to aid comparison. Deep ocean values for GENIE-1 were taken from a model depth of 1700–2500 m.

[b]Estimated from GEOSECS sections [*Bainbridge*, 1981; *Craig et al.*, 1981; *Spencer et al.*, 1982].

[c]Data from *Millero* [2006].

Table 4. Results From Sensitivity Analyses[a]

Variable	Change	ΔDIC_s (%)	ΔDIC_d (%)	ΔALK_s (%)	ΔALK_d (%)	$\Delta CO3_s$ (%)	$\Delta CO3_d$ (%)	ΔH_s^+ (%)
CO_2	+75 μatm	11.8 (17.6)	10.7 (17.5)	9.8 (15.9)	9.7 (15.9)	0.5 (10.3)	0.0 (0.0)	12.4 (7.2)
	−75 μatm	−13.7 (−18.6)	−12.4 (−18.6)	−11.4 (−16.9)	−11.3 (−16.9)	−1.1 (−11.2)	0.0 (0.0)	−14.1 (−9.4)
$\Delta\delta^{13}C$ (F_{mix})	+0.25 per mil	7.6 (n/a)	9.1 (n/a)	8.1 (n/a)	8.3 (n/a)	14.1 (n/a)	0.0 (n/a)	−6.5 (n/a)
	−0.25 per mil	−6.6 (n/a)	−7.9 (n/a)	−7.0 (n/a)	−7.2 (n/a)	−11.8 (n/a)	0.0 (n/a)	6.4 (n/a)
P	+1 × 10^{14} mol/a	4.2 (−0.1)	5.1 (−0.1)	4.5 (−0.1)	4.6 (−0.1)	7.7 (−0.2)	0.0 (0.0)	−3.7 (0.1)
	−1 × 10^{14} mol/a	−4.2 (0.1)	−5.1 (0.1)	−4.5 (0.1)	−4.7 (0.1)	−7.6 (0.3)	0.0 (0.0)	4.0 (−0.1)
T_s	+1°C	−3.8 (−5.3)	−3.4 (−5.3)	−3.1 (−4.8)	−3.1 (−4.8)	0.3 (−2.9)	0.0 (0.0)	3.6 (5.2)
	−1°C	4.0 (5.8)	3.6 (5.8)	3.3 (5.3)	3.3 (5.3)	−0.3 (2.9)	0.0 (0.0)	−3.6 (−5.2)
Ca^{2+}	+1 mmol/kg	−3.1 (−4.5)	−2.9 (−4.5)	−3.2 (−4.7)	−3.2 (−4.7)	−4.4 (−6.9)	−7.7 (−7.7)	2.9 (4.2)
	−1 mmol/kg	3.6 (5.2)	3.3 (5.2)	3.7 (5.4)	3.7 (4.2)	5.3 (8.2)	9.3 (9.3)	−3.2 (−4.5)
r	+0.05	−1.7 (−2.2)	−1.2 (−1.8)	−1.8 (−2.3)	−1.0 (−1.6)	−3.1 (−4.0)	0.0 (0.0)	1.6 (1.9)
	−0.05	1.7 (2.2)	1.1 (1.8)	1.8 (2.4)	1.0 (1.7)	3.1 (4.1)	0.0 (0.0)	−1.5 (−2.1)
MAR_{CaCO3}[b]	−0.073 g/cm^2/ka	1.5 (2.1)	1.3 (2.1)	1.6 (2.2)	1.6 (2.2)	2.7 (3.9)	4.8 (4.8)	−1.3 (−1.9)
	+0.097 g/cm^2/ka	−1.4 (−2.0)	−1.3 (−2.0)	−1.5 (−2.2)	−1.5 (−2.2)	−2.6 (−3.7)	−4.6 (−4.6)	1.3 (1.9)
$CaCO_{3shelf}$[b]	−1.87 × 10^{12} mol/a	1.6 (2.2)	1.4 (2.2)	1.7 (2.4)	1.6 (2.3)	2.9 (4.1)	4.8 (4.8)	−1.4 (−2.0)
	+1.92 × 10^{12} mol/a	−1.5 (−2.2)	−1.4 (−2.1)	−1.6 (−2.3)	−1.6 (−2.3)	−2.8 (−3.9)	−4.6 (−4.6)	1.4 (2.0)
F_{ALK}/F_{DIC}[b,c]	+1.87 × 10^{12} molC/a	1.6 (2.2)	1.4 (2.2)	1.7 (2.4)	1.6 (2.3)	2.9 (4.1)	4.8 (4.8)	−1.4 (−2.0)
	−1.92 × 10^{12} molC/a	−1.5 (−2.2)	−1.4 (−2.1)	−1.6 (−2.3)	−1.6 (−2.3)	−2.8 (−3.9)	−4.6 (−4.6)	1.4 (2.0)
T_d	+1°C	−0.4 (−0.7)	−0.4 (−0.6)	−0.5 (−0.7)	−0.5 (−0.7)	−0.8 (−1.2)	−0.8 (−0.8)	0.4 (0.5)
	−1°C	0.5 (0.7)	0.4 (0.7)	0.5 (0.8)	0.5 (0.8)	0.8 (1.3)	0.8 (0.8)	−0.4 (−0.7)
SO_4^{2-}	+5 mmol/kg	0.3 (0.4)	0.2 (0.4)	0.3 (0.4)	0.3 (0.4)	0.4 (0.6)	0.6 (0.6)	3.2 (3.0)
	−5 mmol/kg	−0.2 (−0.4)	−0.2 (−0.4)	−0.2 (−0.4)	−0.2 (−0.4)	−0.3 (−0.5)	−0.5 (−0.6)	−2.8 (−2.8)
S	+0.25 g/kg	−0.2 (−0.3)	−0.2 (−0.3)	−0.2 (−0.3)	−0.2 (−0.2)	0.0 (0.2)	0.0 (0.0)	0.2 (0.2)
	−0.25 g/kg	0.2 (0.3)	0.2 (0.3)	0.2 (0.3)	0.2 (0.3)	0.1 (0.2)	0.1 (0.1)	−0.3 (−0.5)
Mg^{2+}	+2 mmol/kg	0.0 (0.0)	0.0 (0.0)	0.1 (0.1)	0.1 (0.1)	1.2 (1.2)	2.1 (2.1)	0.2 (0.2)
	−2 mmol/kg	0.0 (0.0)	0.0 (0.0)	−0.1 (−0.1)	−0.1 (−0.1)	−1.2 (−1.2)	−2.1 (−2.1)	−0.2 (−0.2)
$\Delta^{13}Corg$	+0.5 per mil	0.0 (1.2)	0.0 (1.4)	0.0 (1.2)	0.0 (1.3)	0.0 (2.1)	0.0 (0.0)	0.0 (−1.1)
	−0.5 per mil	0.0 (−1.0)	0.0 (−1.3)	0.0 (−1.1)	0.0 (−1.1)	0.0 (−1.9)	0.0 (0.0)	0.0 (0.9)

[a]Each variable was changed in isolation and the results displayed as a percentage change relative to the Holocene steady state. The values in parentheses represent the percentage change following the adjustment of F_{mix} until Holocene values of $\Delta\delta^{13}C$ were reached.
[b]These variables were adjusted by the amount required to change the CCD by ±250 m.
[c]F_{ALK}:F_{DIC} was changed in a 2:1 ratio.

[33] When CO_2 was kept constant, DIC and alkalinity both showed an increase during the last 20 Ma (Figures 5a, 5b, 5d, and 5e) due to geological evidence for a steady decrease in the Ca^{2+} concentration of the ocean and an increase in the depth of the CCD, both of which are model boundary conditions. Both of these factors caused an increase in deep ocean CO_3^{2-} concentration which, at a constant level of atmospheric CO_2, could only be sustained with higher concentrations of DIC and alkalinity.

4.4.2. CO_3^{2-}

[34] Equilibrium surface ocean CO_3^{2-} showed very limited sensitivity to different CO_2 histories but a strong sensitivity to changes in $\Delta\delta^{13}C$. However, deep ocean CO_3^{2-} showed no sensitivity to either CO_2 or $\Delta\delta^{13}C$. For these reasons, proxy reconstructions of surface ocean CO_3^{2-} are of limited use for constraining the long-term evolution of CO_2 as changes to CO_3^{2-} would likely be reflecting variance in processes that control vertical gradients in the ocean, and not changes to CO_2.

[35] The background increase in both deep and surface ocean CO_3^{2-} for all four CO_2 histories was caused by the changes to Mg^{2+} and Ca^{2+} and the deepening of the CCD. This trend was consistent with previous reconstructions of surface ocean CO_3^{2-} [*Demicco et al.*, 2003; *Tyrrell and Zeebe*, 2004]. This agreement was not unexpected as we used the same records for seawater Mg^{2+} and Ca^{2+} as *Tyrrell and Zeebe* [2004]. Any further discrepancies between the reconstructions are due to the different assumptions made regarding vertical gradients in the ocean, the different approaches to the estimation of constants, and error propagation. However, since the first-order control on the evolution of CO_3^{2-} is Ca^{2+} concentration, the major trends are shared between all reconstructions. The surface ocean CO_3^{2-} reconstruction of *Demicco et al.* [2003] is almost uniformly offset from the reconstructions presented here by 50 μmol/kg because they used an average surface CO_3^{2-} of 250 μmol/kg at 0 Ma, rather than the ∼200 μmol/kg used in this study.

4.4.3. Surface Ocean pH

[36] From our results we infer that if CO_2 did covary with temperature and ice volume over the last 20 Ma, then we would expect to see an increase in surface ocean pH over this same interval. However, this result fits poorly with existing constraints on surface ocean pH, which display a relatively flat trend [*Pearson and Palmer*, 2000]. Even if CO_2 is kept constant, modeled surface ocean pH increases by up to 0.1 pH units during the last 20 Ma. This background trend is a robust feature of the geological constraints on Ca^{2+}, the CCD and surface ocean temperature.

[37] When $\Delta\delta^{13}C$ was used as a constraint, the best agreement between model and proxy pH was for an increasing CO_2 during the last 20 Ma. (Figure 6f). However, if we ignore the record of $\Delta\delta^{13}C$ and assume Holocene values for biological productivity and ocean overturning, proxy estimates for pH and CO_2 are consistent with each other (Figure 8f).

4.4.4. Weathering Rates

[38] We modeled a ∼25% increase in "net weathering" rates over the last 20 Ma (Figure 9b). This was a direct consequence of the record of deepening CCD we used

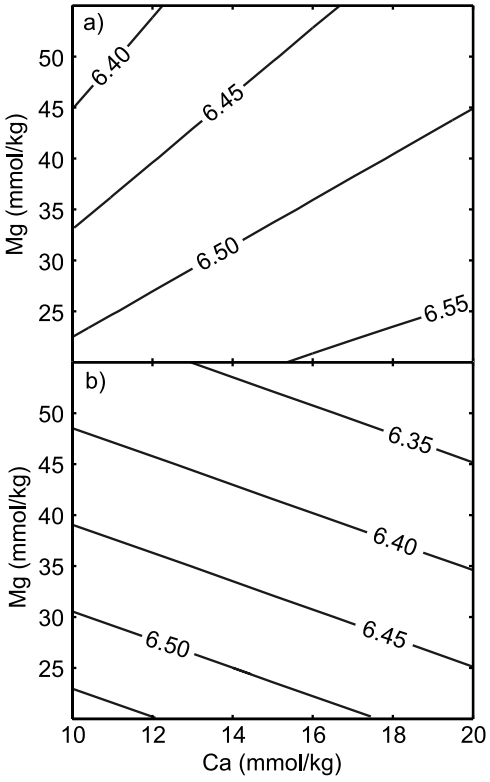

Figure 4. Comparison of two methods for estimating pK_{sp} at different concentrations of Mg^{2+} and Ca^{2+}. Each plot is contoured for pK_{sp}, and calculations were made for T = 25°C and S = 35‰ (when Ca^{2+} = 10 mmol/kg and Mg^{2+} = 52.82 mmol/kg). (a) pK_{sp} estimated with an empirical relationship [*Tyrrell and Zeebe*, 2004] derived from an experimental data set for which only Mg^{2+} was varied [*Mucci and Morse*, 1984]. (b) pK_{sp} estimated using a Pitzer chemical equilibrium model [*Millero and Pierrot*, 1998].

as a model boundary condition. As we earlier discussed (sections 3.1.4. and 4.3.), this increase could be a result of changes either in global weathering rates, pelagic mass accumulation rates, or the fraction of $CaCO_3$ sedimentation occurring in coastal regions. However, given the trend of global cooling and increased ice volume in the last 20 Ma, we interpret the deepening of the CCD and the modeled increase in "net weathering" to be a result of decreased coastal $CaCO_3$ sedimentation and not an increase in global weathering rates. This follows the reasoning of *Kump and Arthur* [1997] who concluded that deepening of the CCD during the Cenozoic was predominantly due to changes in the partitioning of $CaCO_3$ accumulation between the deep ocean and continental shelves and that [*Kump and Arthur*, 1997, p. 417] "factors such as fluctuations in riverine alkalinity delivery or vertical accumulation rates have been of secondary importance."

4.4.5. Global Productivity

[39] All the results we have presented so far have interpreted $\Delta\delta^{13}C$ as a constraint on F_{mix} while biological productivity (P) was kept constant. In order to estimate changes in P we repeated our simulations using $\Delta\delta^{13}C$ as a constraint on global productivity while F_{mix} was kept constant. Despite this change in methodology, all values for calculated variables changed by less than 1.5%. This was expected as we have already demonstrated the near perfect trade-off between F_{mix} and P (see section 4.3). This second set of simulations shows that in the absence of changes to ocean circulation, our record of $\Delta\delta^{13}C$ is consistent with a broad minimum in productivity at ~15 Ma (Figure 9c). However, *Föllmi* [1995] reports a significant maximum in global oceanic phosphorus accumulation rates also at ~15 Ma. This suggests that either our compilation of $\Delta\delta^{13}C$ is unrepresentative of global changes, or that changes in $\Delta\delta^{13}C$ are also recording variability in ocean mixing and circulation, not just variations in productivity.

5. Discussion

5.1. Consequences for the Relationship Between CO_2 and Climate

[40] The proxy estimates for CO_2 we used for the last 20 Ma exhibit a relatively flat trend with reported mean values between 200 and 325 μatm [*Pagani et al.*, 2005a]. These data are seemingly at odds with composite records of climate and ice volume [e.g., *Zachos et al.*, 2001] that show a trend toward cooler temperatures and increased ice volume. Of all the CO_2 histories tested in this study, the linear decrease of atmospheric CO_2 from 556 μatm to 278 μatm is the most compatible with the climate record for the last 20 Ma, but the least consistent with the proxy pH data. The proxy CO_2 reconstruction and a linear increase in CO_2 are apparently the most compatible with the proxy pH data. However, these reconstructions are the least compatible with a history of global cooling and increased ice volume.

[41] Because the system we have studied is underconstrained, there is no unique solution for atmospheric CO_2 for a given reconstruction of surface ocean pH. Despite this uncertainty, by making reasonable assumptions regarding ocean turnover and biological productivity we conclude that if CO_2 was strongly coupled to temperature and ice volume over the last 20 Ma, predicted values of surface ocean pH fit poorly with current proxy reconstructions. This suggests that if the published boron isotope-based pH reconstructions are robust (see *Hönisch et al.* [2007], *Pagani et al.* [2005b], and *Pagani and Spivack* [2007] for recent discussion of the boron isotope proxy of pH), a mechanism other than declining CO_2 must have been responsible for global cooling during the last 20 Ma.

5.2. A Carbon Cycle Model as a Tool for Making Independent Estimates of CO_2 From pH

[42] Past studies have attempted to estimate atmospheric CO_2 from proxy reconstructions of surface ocean pH by making assumptions regarding the evolution of ocean DIC or alkalinity. These reconstructions of CO_2 are only as valid (and accurate) as the assumed values for alkalinity or DIC used in the calculations. In the absence of other constraints on the carbonate system, one way of directly inferring atmospheric CO_2 values from proxy constraints on surface water pH is with a carbon cycle model such as the one

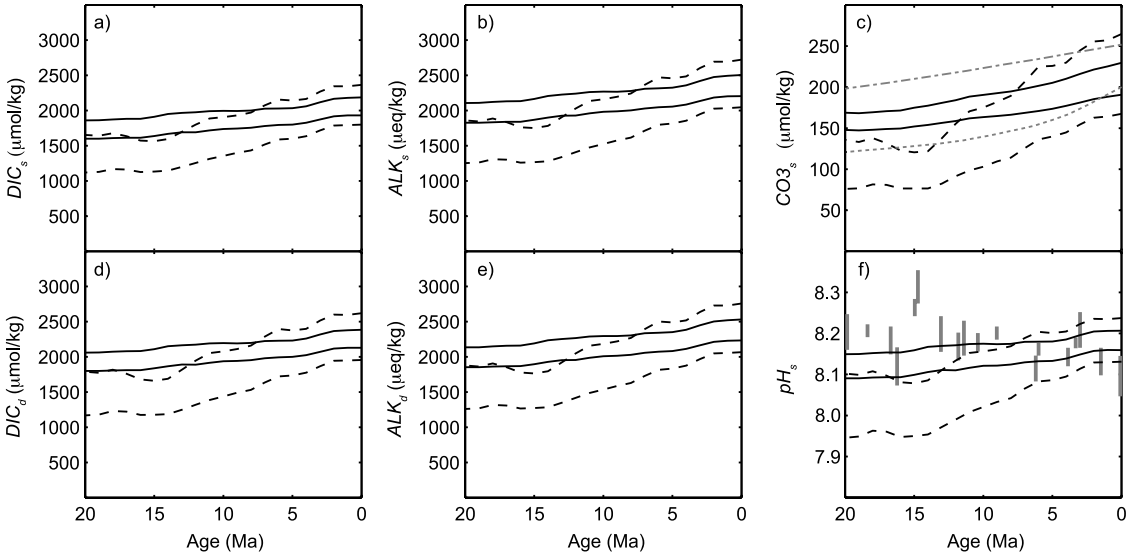

Figure 5. Model results for constant CO_2 (278 μatm). Solid black lines were calculated using constant values of biological productivity and ocean overturning. Dashed black lines were calculated using $\Delta\delta^{13}C$ as a constraint. (a) Surface ocean DIC. (b) Surface alkalinity. (c) Calculated surface CO_3^{2-} and previous model reconstructions of surface ocean CO_3^{2-} by *Tyrrell and Zeebe* [2004] (gray dotted line) and *Demicco et al.* [2003] (gray dot-dashed line). (d) Deep ocean DIC. (e) Deep ocean alkalinity. (f) Calculated surface ocean pH and ranges of proxy estimates (total pH scale) [*Pearson and Palmer*, 2000] (gray bars).

presented in this study. If geological constraints can be used to estimate boundary conditions, a tuning process could then be used to determine the values for atmospheric CO_2, DIC, alkalinity, and CO_3^{2-} that are most consistent with the proxy estimate of pH. The uncertainty in these values would be dependent on how precisely model boundary conditions can be constrained, and would be especially sensitive to any assumptions made regarding ocean overturning and biological productivity.

5.3. Caveats

5.3.1. Model Simplicity

[43] This model could potentially be improved by increasing the number of boxes in order to differentiate between the high- and low-latitude surface oceans, thereby creating a model configuration similar to models used to investigate interglacial-glacial variations in CO_2 [e.g., *Knox and McElroy*, 1984; *Sarmiento and Toggweiler*, 1984; *Siegenthaler and Wenk*, 1984]. Such a modification would

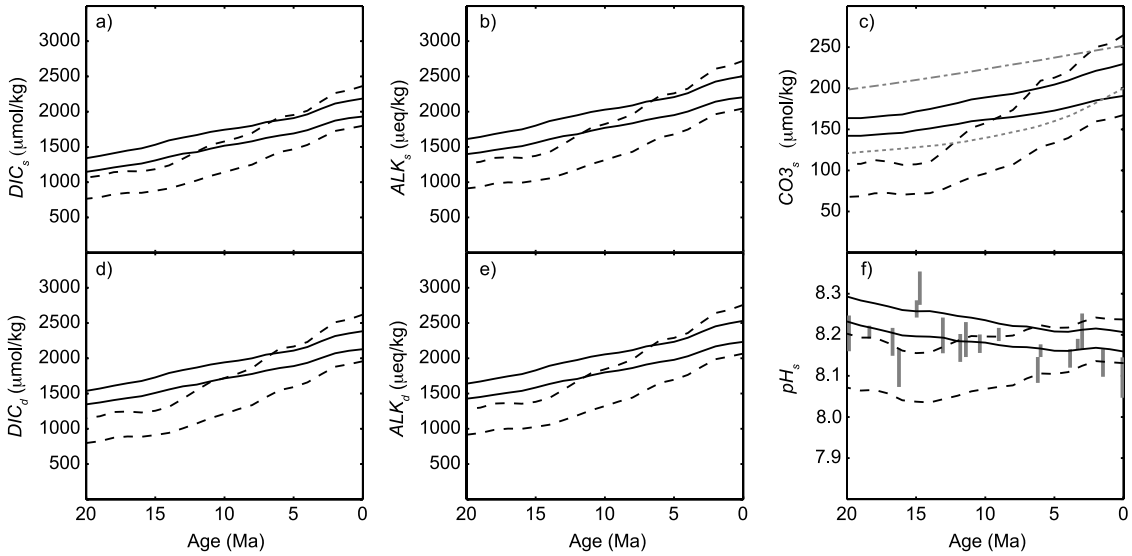

Figure 6. Model results for rising CO_2 between 20 and 0 Ma (doubling from 139 to 278 μatm). See Figure 5 for descriptions.

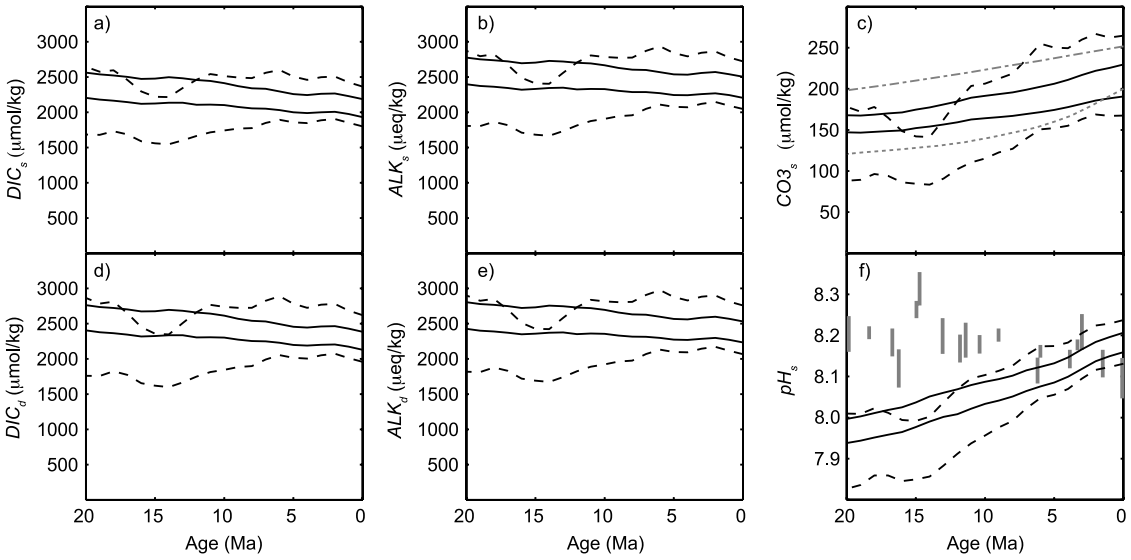

Figure 7. Model results for declining CO_2 between 20 and 0 Ma (halving from 556 to 278 μatm). See Figure 5 for descriptions.

allow direct comparison of model and measured $\Delta\delta^{13}C$ gradients from the low latitudes, without the need for correcting the measured data to "global" values.

[44] Explicitly tracing more variables (e.g., Ca^{2+}, Mg^{2+}, nutrients, O_2) would also help to reduce the potential parameter space for model boundary conditions by allowing us to identify unrealistic scenarios (e.g., negative nutrient concentrations or the presence/absence of ocean anoxia). An even more rigorous approach would be to use a fully coupled earth system model that includes both 3-D ocean and biochemistry components (e.g., GENIE-1).

[45] Mechanistically linking parameters such that there are fewer independent variables (e.g., coupling together weathering fluxes of phosphorus, alkalinity, DIC, Ca^{2+}, Mg^{2+}) may also provide further constraints on the system. However, including these variables would require a very different modeling methodology, particularly with regard to modeling Mg^{2+} and Ca^{2+}. The long residence times of Mg^{2+} and Ca^{2+} requires there to have been imbalance in the sources and sinks of Mg^{2+} and Ca^{2+} for millions of years to cause the trends witnessed through the Cenozoic. However, the ocean's limited capacity for alkalinity storage [*Kump and Arthur*, 1997] and the time scale of carbonate compensation (~50 ka) mean that this imbalance would have to be sustained without long-term imbalance in the alkalinity cycle. An imbalance in the Mg^{2+} and Ca^{2+} cycles

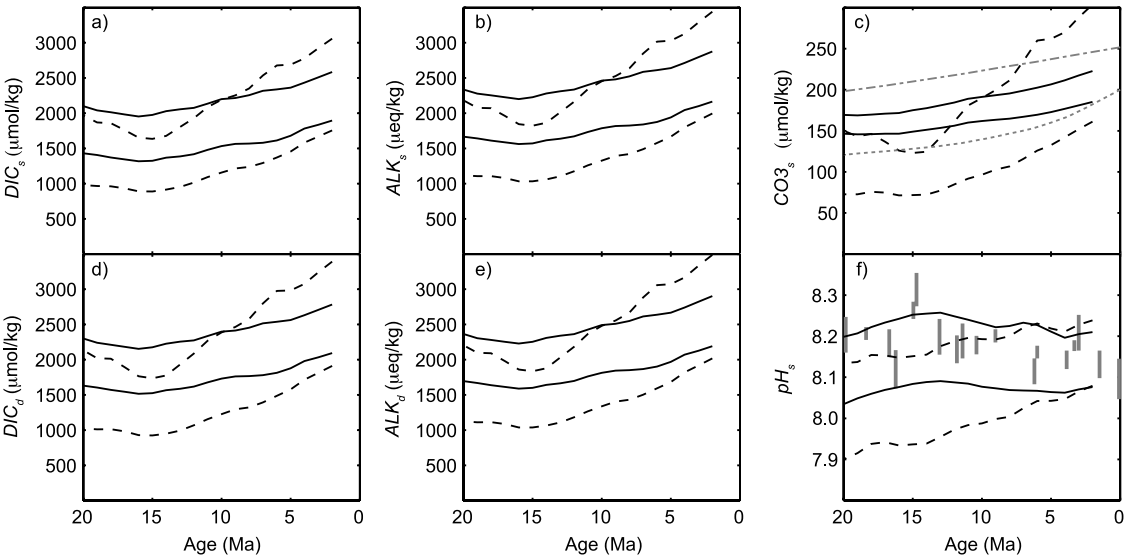

Figure 8. Model results for the CO_2 history derived from proxy data. See Figure 5 for descriptions.

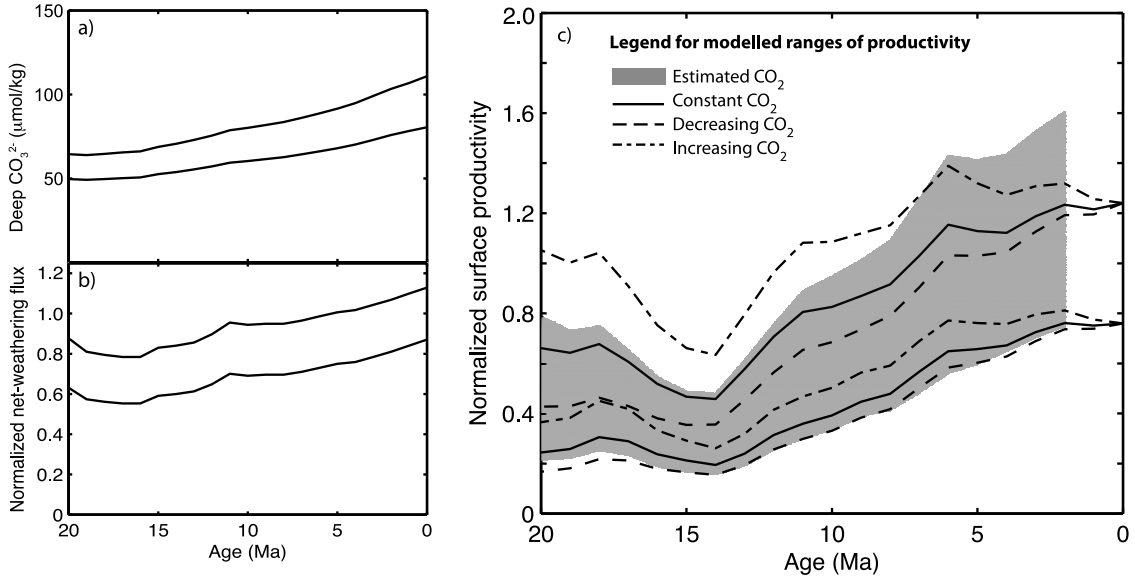

Figure 9. (a) Calculated record of deep ocean CO_3^{2-} valid for all CO_2 histories and all $\Delta\delta^{13}C$ gradients. (b) Modeled changes to "net weathering" consistent with geological constraints on the CCD. (c) Modeled ranges of productivity when $\Delta\delta^{13}C$ was assumed to constrain productivity and F_{mix} was kept constant (see section 4.4.5).

may have been achieved by changes in the fraction of alkalinity sourced from the weathering of Mg silicates and $MgCO_3$. Modeling such a scenario would require significant changes to our modeling methodology. For example, the assumption of steady state we have made for each of our time slices would no longer be viable.

5.3.2. Temporal Resolution

[46] The main processes that control CO_2 on the longest geological time scales are thought to be the volcanic and metamorphic out-gassing of CO_2, the drawdown of CO_2 during the weathering of silicate rocks, the burial of carbon in ocean sediments, and the weatherability of silicate rocks as a function of climate [e.g., *Berner et al.*, 1983; *Kump and Arthur*, 1997; *Kump et al.*, 2000]. Because the geochemical weathering cycle and CO_2 degassing control the long-term evolution of CO_2, mechanisms such as oceanic and biological processes can only be responsible for variability on time scales shorter than that of the silicate weathering feedback (~0.5 Ma). The results presented here were purposefully calculated at a resolution to extract trends on a million year time scale. This study was not intended to reveal the variance present on time scales shorter than a million years, and hence such variability will not have been captured by these calculations.

[47] It is also worth noting that any measurements made with a sampling resolution much lower than the variability present in nature will always be aliased. It is likely that there was more variability in surface water pH than is captured by the low-resolution surface ocean pH record of *Pearson and Palmer* [2000]. For this reason, these pH "snapshots" do not necessarily correspond to the long-term means calculated for this study. Unfortunately, the low resolution of the existing proxy records means there is an inherent uncertainty in assessing which records are (and are not) consistent with one another. Until records of pH are developed at higher resolution, and from other proxies, the interpretation and comparison of these records should be undertaken with caution.

6. Conclusions

[48] A simple model of the carbon cycle and geological data were used to reconstruct the oceanic carbonate system (DIC, alkalinity, CO_3^{2-}, and pH) for four different histories of CO_2 covering the last 20 Ma. Results for the Holocene agreed well with measured hydrographic data and with results from a more complex model (GENIE-1). Results for the LGM were consistent with proxy reconstructions of surface ocean pH. Sensitivity testing demonstrated that CO_2, Ca^{2+} concentration, surface ocean temperature, biological productivity and ocean overturning had the largest influence on model calculations. In addition, total salinity was shown to be less important than the relative abundance of individual elements in seawater.

[49] The poorly constrained nature of the system we have studied meant that multiple CO_2 histories could be invoked to explain the same pH trend depending on the assumptions made regarding ocean overturning and biological productivity. However, when we assumed that CO_2 was strongly coupled to temperature and ice volume over the last 20 Ma, the predicted values of surface ocean pH did not fit with current proxy reconstructions of surface ocean pH. If boron isotope based estimates of pH are robust, an alternative explanation to decreasing levels of atmospheric CO_2 is required to explain trends of global cooling. New constraints on surface ocean pH and/or CO_2 are needed to test this hypothesis.

Appendix A: Carbonate System in Seawater

[50] The amount of CO_2 that dissolves in the surface ocean is proportional to the partial pressure of CO_2 in the atmosphere, and is described by Henry's Law. The balance of the equilibrium is determined by the solubility of CO_2 in water (k_{CO2}). $CO_{2(aq)}$ reacts with water to form bicarbonate (HCO_3^-) and hydrogen ions and is characterized with an equilibrium constant (k_1).

$$CO_{2(aq)} + H_2O \leftrightarrow H^+ + HCO_3^-$$

Some HCO_3^- ions undergo further dissociation to form carbonate ions (CO_3^{2-}) allowing another constant (k_2) to be defined.

$$HCO_3^- \leftrightarrow H^+ + CO_3^{2-}$$

Total dissolved inorganic carbon (DIC) is the sum of the three species of dissolved CO_2 present in seawater.

$$[DIC] = [CO_2] + \left[HCO_3^-\right] + \left[CO_3^{2-}\right]$$

Alkalinity can be defined as the excess positive charge from conservative ions in seawater (such as Na^+, K^+, Cl^-, Mg^{2+}, Ca^{2+}, and SO_4^{2-}) that must be balanced by the anions of weak acids such as HCO_3^-. For most purposes, including natural seawater, "practical alkalinity" (defined below) can be used as an approximation for total alkalinity [*Zeebe and Wolf-Gladrow*, 2001].

$$[ALK] = \left[HCO_3^-\right] + 2\left[CO_3^{2-}\right] + \left[B(OH)_4^-\right] + [OH^-] - [H^+]$$

Notice that CO_3^{2-} contributes two equivalents of alkalinity because it is a doubly charged ion.

Appendix B: Calculation of Constants

[51] Constants may be calculated as a function of solution composition and temperature either with simple empirical relationships [e.g., *Ben-Yaakov and Goldhaber*, 1973; *Tyrrell and Zeebe*, 2004] or by using theoretical models that consider the interactions between all the ionic species within a solution [e.g., *Millero and Pierrot*, 1998]. We considered the theoretical modeling approach to be the most robust, and a Pitzer chemical equilibrium model [*Millero and Pierrot*, 1998] was used to calculate all constants as a function of the temperature and the ionic composition of seawater. The relationships described by *Millero* [1995] were used to evaluate the effect of pressure on equilibrium constants.

Appendix C: Statistical Methods

[52] In order to extract long-term trends and estimate uncertainty, data were smoothed using a nonparametric regression technique [*Poore et al.*, 2006] and bias-corrected 95% confidence bands were calculated around regression estimates following *Xia* [1998] and *Samworth and Poore* [2005]. Regression curves were calculated using a local linear kernel estimator with a constant bandwidth of 2 Ma. This bandwidth controlled the width of an Epanechnikov kernel (K) of the form: $K = (3/4h) \cdot (1 - (x/h)^2)$, where h is the half-width, or bandwidth of the kernel. The regression process required each point on the smoothed curve to be locally fitted with a weighted least squares regression line, with the weighting determined by the height of the kernel centered on that point. The weighting process ensured that those data closest to the center of the kernel had more influence on the regression estimate than those further away. The bandwidth of the kernel determined the relative weightings, with larger bandwidths affording more influence to data further from the point of evaluation. The bias in the confidence bands, particularly noticeable at peaks and troughs, was corrected using a bandwidth of 1 Ma for the Epanechnikov kernel. This process resulted in confidence bands that varied smoothly but that better reflected the likely value of the true regression function at any given point.

Notation

ALK_d	deep ocean alkalinity concentration, eq/kg.
ALK_s	surface ocean alkalinity concentration, eq/kg.
$CaCO3_{pelagic}$	sediment flux of $CaCO_3$ in the deep ocean, mol/a.
$CaCO3_{shelf}$	sediment flux of $CaCO_3$ on the continental shelf, mol/a.
$CO3_d$	deep ocean carbonate ion concentration, mol/kg.
$CO3_s$	surface ocean carbonate ion concentration, mol/kg.
$Corg_{pelagic}$	sediment flux of organic carbon in the deep ocean, mol/a.
$Corg_{shelf}$	sediment flux of organic carbon on the continental shelf, mol/a.
DIC_d	deep ocean dissolved inorganic carbon concentration, mol/kg.
DIC_s	surface ocean dissolved inorganic carbon concentration, mol/kg.
$F_{air\text{-}sea}$	flux of carbon from the atmosphere to the surface ocean, mol/a.
F_{ALK}	riverine flux of alkalinity, mol/a.
F_{DIC}	riverine flux of dissolved inorganic carbon, mol/a.
F_{mix}	ocean overturning flux, kg/a.
F_{NO3}	riverine flux of nitrates (balancing loss to organic sediments), mol/a.
MAR_{CaCO3}	average $CaCO_3$ mass accumulation rate above the CCD, g/cm^2/ka.
M_{CO2}	mass of carbon in the atmosphere, moles.
M_d	mass of the deep ocean, kg.
M_s	mass of the surface ocean, kg.
P	biological productivity in the surface ocean, molCorg/a.
pH_d	deep ocean pH.
pH_s	surface ocean pH.
r	ratio of $CaCO_3$/organic carbon productivity.

S	salinity of the ocean, g/kg.
T_d	deep ocean temperature, °C.
T_s	surface ocean temperature, °C.
$\delta^{13}C_d$	carbon isotope composition of the deep ocean, per mil.
$\delta^{13}C_{riv}$	carbon isotope composition of rivers, per mil.
$\delta^{13}C_s$	carbon isotope composition of the surface ocean, per mil.
$\Delta Corg$	isotopic fractionation of carbon during photosynthesis, per mil.
$\Delta\delta^{13}C$	carbon isotope gradient between the surface and deep ocean, per mil.

[53] **Acknowledgments.** We acknowledge financial support from the Natural Environment Research Council (studentship NER/S/A/2006/14070). A. Tripati was supported by a NERC postdoctoral fellowship and a Magdalene College Junior Research Fellowship. We thank H. Poore and F. Millero for discussing this work and providing us with code, M. Bickle for discussions, and M. Leckie and S. Nathan for providing us with Mg/Ca data. Constructive reviews from T. Lenton and one other anonymous reviewer improved this manuscript.

References

Bainbridge, A. E. (1981), *GEOSECS Atlantic Expedition*, vol. 2, *Sections and Profiles*, Natl. Sci. Found., Washington, D. C.

Ben-Yaakov, S., and M. B. Goldhaber (1973), The influence of sea water composition on the apparent constants of the carbonate system, *Deep Sea Res.*, *20*, 87–99.

Bergman, N. M., et al. (2004), COPSE: A new model of biogeochemical cycling over phanerozoic time, *Am. J. Sci.*, *304*, 397–437, doi:10.2475/ajs.304.5.397.

Berner, R. A., and Z. Kothavala (2001), GEOCARB III: A revised model of atmospheric CO_2 over phanerozoic time, *Am. J. Sci.*, *301*, 182–204, doi:10.2475/ajs.301.2.182.

Berner, R. A., et al. (1983), The carbonate-silicate geochemical cycle and its effect on atmospheric carbon-dioxide over the past 100 million years, *Am. J. Sci.*, *283*, 641–683.

Billups, K., and D. P. Schrag (2002), Paleotemperatures and ice volume of the past 27 Myr revisited with paired Mg/Ca and $^{18}O/^{16}O$ measurements on benthic foraminifera, *Paleoceanography*, *17*(1), 1003, doi:10.1029/2000PA000567.

Billups, K., et al. (1999), Link between oceanic heat transport, thermohaline circulation, and the Intertropical Convergence Zone in the early Pliocene Atlantic, *Geology*, *27*, 319–322, doi:10.1130/0091-7613(1999)027<0319:LBOHTT>2.3.CO;2.

Boyd, P. W., and T. W. Trull (2007), Understanding the export of biogenic particles in oceanic waters: Is there consensus?, *Prog. Oceanogr.*, *72*, 276–312, doi:10.1016/j.pocean.2006.10.007.

Broecker, W. S., and T.-H. Peng (1982), *Tracers in the Sea*, Lamont-Doherty Geol. Obs., Palisades, N. Y,.

Caldeira, K., and M. E. Wickett (2003), Anthropogenic carbon and ocean pH, *Nature*, *425*, 365, doi:10.1038/425365a.

Cerling, T. E. (1991), Carbon-dioxide in the atmosphere—Evidence from Cenozoic and Mesozoic paleosols, *Am. J. Sci.*, *291*, 377–400.

Cheng, X., et al. (2004a), Data report: Stable isotopes from Site 1143 [online], *Proc. Ocean Drill. Program Sci. Results*, 184, 8 pp., (Available at http://www-odp.tamu.edu/publications/184_SR/VOLUME/CHAPTERS/221.PDF).

Cheng, X., et al. (2004b), Data report: Stable isotopes from Sites 1147 and 1148 [online], *Proc. Ocean Drill. Program Sci. Results*, 184, 12 pp., (Available at http://www-odp.tamu.edu/publications/184_SR/VOLUME/CHAPTERS/223.PDF).

Clemens, S. C., and W. L. Prell (2003), Data report: Oxygen and carbon isotopes from Site 1146, northern South China Sea [online], *Proc. Ocean Drill. Program Sci. Results*, 184, 8 pp., (Available at http://www-odp.tamu.edu/publications/184_SR/VOLUME/CHAPTERS/214.PDF).

Collier, R., and J. Edmond (1984), The trace-element geochemistry of marine biogenic particulate matter, *Prog. Oceanogr.*, *13*, 113–199, doi:10.1016/0079-6611(84)90008-9.

Craig, H., et al. (1981), *GEOSECS Pacific Ocean Expedition*, vol. 4, *Sections and Profiles*, Natl. Sci. Found, Washington, D. C.

Delaney, M. L., and E. A. Boyle (1988), Tertiary paleoceanic chemical variability: Unintended consequences of simple geochemical models, *Paleoceanography*, *3*, 137–156, doi:10.1029/PA003i002p00137.

Demicco, R. V., et al. (2003), Atmospheric pCO_2 since 60 Ma from records of seawater pH, calcium, and primary carbonate mineralogy, *Geology*, *31*, 793–796, doi:10.1130/G19727.1.

Dickson, J. A. D. (2002), Fossil echinoderms as monitor of the Mg/Ca ratio of Phanerozoic oceans, *Science*, *298*, 1222–1224, doi:10.1126/science.1075882.

Edmond, J. M., et al. (1979), Ridge crest hydrothermal activity and the balances of the major and minor elements in the ocean: The Galapagos data, *Earth Planet. Sci. Lett.*, *46*, 1–18, doi:10.1016/0012-821X(79)90061-X.

Emerson, S., and M. Bender (1981), Carbon fluxes at the sediment-water interface of the deep sea: Calcium-carbonate preservation, *J. Mar. Res.*, *39*, 139–162.

Flower, B. P., and J. P. Kennett (1995), Middle Miocene deepwater paleoceanography in the southwest Pacific: Relations with East Antarctic Ice Sheet development, *Paleoceanography*, *10*, 1095–1112, doi:10.1029/95PA02022.

Föllmi, K. B. (1995), 160 m. y. record of marine sedimentary phosphorus burial: Coupling of climate and continental weathering under greenhouse and icehouse conditions, *Geology*, *23*, 503–506, doi:10.1130/0091-7613(1995)023<0503:MYROMS>2.3.CO;2.

Gasperi, J. T., and J. P. Kennett (1993), Miocene planktonic foraminifers at DSDP site 289: Depth stratification using isotopic differences, *Proc. Ocean Drill. Program Sci. Results*, *130*, 323–332.

Gradstein, F., et al. (2004), *A Geological Time Scale 2004*, Cambridge Univ. Press, Cambridge, U. K.

Hayes, J. M., et al. (1999), The abundance of C^{13} in marine organic matter and isotopic fractionation in the global biogeochemical cycle of carbon during the past 800 Ma, *Chem. Geol.*, *161*, 103–125, doi:10.1016/S0009-2541(99)00083-2.

Hönisch, B., and N. G. Hemming (2005), Surface ocean pH response to variations in pCO_2 through two full glacial cycles, *Earth Planet. Sci. Lett.*, *236*, 305–314, doi:10.1016/j.epsl.2005.04.027.

Hönisch, B., et al. (2007), Comment on "A critical evaluation of the boron isotope-pH proxy: The accuracy of ancient pH estimates" by M. Pagani, D. Lemarchand, A. Spivack and J. Gaillardet, *Geochim. Cosmochim. Acta*, *71*, 1636–1641, doi:10.1016/j.gca.2006.07.045.

Horita, J., et al. (2002), Chemical evolution of seawater during the Phanerozoic: Implications from the record of marine evaporites, *Geochim. Cosmochim. Acta*, *66*, 3733–3756, doi:10.1016/S0016-7037(01)00884-5.

Jin, X., et al. (2006), Diagnosing the contribution of phytoplankton functional groups to the production and export of particulate organic carbon, $CaCO_3$, and opal from global nutrient and alkalinity distributions, *Global Biogeochem. Cycles*, *20*, GB2015, doi:10.1029/2005GB002532.

Keigwin, L., and G. Keller (1984), Middle Oligocene cooling from equatorial Pacific DSDP site-77B, *Geology*, *12*, 16–19, doi:10.1130/0091-7613(1984)12<16:MOCFEP>2.0.CO;2.

Knox, F., and M. B. McElroy (1984), Changes in atmospheric CO_2: Influence of the marine biota at high latitude, *J. Geophys. Res.*, *89*, 4629–4637, doi:10.1029/JD089iD03p04629.

Kroopnick, P. M. (1985), The distribution of C^{13} of \sum\nolimits$\sum CO_2$ in the world oceans, *Deep Sea Res.*, *32*, 57–84, doi:10.1016/0198-0149(85)90017-2.

Kump, L. R., and M. A. Arthur (1997), Global chemical erosion during the Cenozoic: Weatherability balances the budget, in *Tectonic Uplift and Climate Change*, edited by W. Ruddiman, pp. 399–426, Plenum, New York.

Kump, L. R., et al. (2000), Chemical, weathering, atmospheric CO_2, and climate, *Annu. Rev. Earth Planet. Sci.*, *28*, 611–667, doi:10.1146/annurev.earth.28.1.611.

Kurschner, W. M., et al. (1996), Oak leaves as biosensors of late Neogene and early Pleistocene paleoatmospheric CO_2 concentrations, *Mar. Micropaleontol.*, *27*, 299–312, doi:10.1016/0377-8398(95)00067-4.

Lasaga, A. C., et al. (1985), An improved geochemical model of atmospheric CO_2 over the past 100 million years, in *The Carbon Cycle and Atmospheric CO_2: Natural Variations Archean to Present*, *Geophys. Monogr. Ser.*, vol. 32, edited by E. T. Sundquist and W. S. Broecker, pp. 397–411, AGU, Washington, D. C.

Lear, C. H., et al. (2000), Cenozoic deep-sea temperatures and global ice volumes from Mg/Ca in benthic foraminiferal calcite, *Science*, *287*, 269–272, doi:10.1126/science.287.5451.269.

Lenton, T. M., et al. (2006), Millennial timescale carbon cycle and climate change in an efficient Earth system model, *Clim. Dyn.*, *26*(7), 687–711.

Lowenstein, T. K., et al. (2001), Oscillations in Phanerozoic seawater chemistry: Evidence from fluid inclusions, *Science*, *294*, 1086–1088, doi:10.1126/science.1064280.

Luthi, D., et al. (2008), High-resolution carbon dioxide concentration record 650,000–800,000 years before present, *Nature*, *453*, 379–382, doi:10.1038/nature06949.

Lyle, M. (2003), Neogene carbonate burial in the Pacific Ocean, *Paleoceanography*, *18*(3), 1059, doi:10.1029/2002PA000777.

Menard, H. W., and S. M. Smith (1966), Hypsometry of ocean basin provinces, *J. Geophys. Res.*, *71*, 4305–4325.

Miller, K. G., and R. G. Fairbanks (1985), Oligocene to Miocene global carbon isotope cycles and abyssal circulation changes, in *The Carbon Cycle and Atmospheric CO2: Natural Variations Archean to Present*, *Geophys. Monogr. Ser.*, vol. 32, edited by E. T. Sundquist and W. S. Broecker, pp. 469–486, AGU, Washington, D. C.

Millero, F. J. (1995), Thermodynamics of the carbon-dioxide system in the oceans, *Geochim. Cosmochim. Acta*, *59*, 661–677, doi:10.1016/0016-7037(94)00354-O.

Millero, F. J. (2006), *Chemical Oceanography*, 3rd ed., Taylor and Francis, New York.

Millero, F. J., and D. Pierrot (1998), A chemical equilibrium model for natural waters, *Aquat. Geochem.*, *4*, 153–199, doi:10.1023/A:1009656023546.

Mix, A. C., et al. (1995), Benthic foraminifer stable isotope record from site 849 (0–5 Ma): Local and global climate changes, *Proc. Ocean Drill. Program Sci. Results*, *138*, 371–412.

Morse, J. W., and R. S. Arvidson (2002), The dissolution kinetics of major sedimentary carbonate minerals, *Earth Sci. Rev.*, *58*, 51–84, doi:10.1016/S0012-8252(01)00083-6.

Mucci, A., and J. W. Morse (1984), The solubility of calcite in seawater solutions of various magnesium concentration, I_t = 0.697 m at 25°C and one atmosphere total pressure, *Geochim. Cosmochim. Acta*, *48*, 815–822, doi:10.1016/0016-7037(84)90103-0.

Pagani, M., and A. Spivack (2007), Response to the comment by B. Hönisch, N. G. Hemming, B. Loose on "A critical evaluation of the boron isotop-pH proxy: The accuracy of ancient ocean pH estimates", *Geochim. Cosmochim.*, *71*, 1642, doi:10.1016/j.gca.2006.11.035.

Pagani, M., et al. (1999), Miocene evolution of atmospheric carbon dioxide, *Paleoceanography*, *14*, 273–292, doi:10.1029/1999PA900006.

Pagani, M., et al. (2005a), Marked decline in atmospheric carbon dioxide concentrations during the Paleogene, *Science*, *309*, 600–603, doi:10.1126/science.1110063.

Pagani, M., et al. (2005b), A critical evaluation of the boron isotope-pH proxy: The accuracy of ancient ocean pH estimates, *Geochim. Cosmochim. Acta*, *69*, 953–961, doi:10.1016/j.gca.2004.07.029.

Pearson, P. N., and M. R. Palmer (1999), Middle eocene seawater pH and atmospheric carbon dioxide concentrations, *Science*, *284*, 1824–1826, doi:10.1126/science.284.5421.1824.

Pearson, P. N., and M. R. Palmer (2000), Atmospheric carbon dioxide concentrations over the past 60 million years, *Nature*, *406*, 695–699, doi:10.1038/35021000.

Pearson, P. N., and N. J. Shackleton (1995), Neogene multispecies planktonic foraminifer stable isotope record, site 871, Limalok Guyot, *Proc. Ocean Drill. Program Sci. Results*, *144*, 401–410.

Petit, J. R., et al. (1999), Climate and atmospheric history of the past 420,000 years from the Vostok ice core, Antarctica, *Nature*, *399*, 429–436, doi:10.1038/20859.

Poore, H. R., et al. (2006), Neogene overflow of Northern Component Water at the Greenland-Scotland Ridge, *Geochem. Geophys. Geosyst.*, *7*, Q06010, doi:10.1029/2005GC001085.

Ridgwell, A., et al. (2007), Marine geochemical data assimilation in an efficient Earth System Model of global biogeochemical cycling, *Biogeosciences*, *4*, 87–104.

Royer, D. L. (2003), Estimating latest Cretaceous and Tertiary atmospheric CO2 from stomatal indices, in *Causes and Consequences of Globally Warm Climates in the Early Paleogene*, edited by S. L. Wing et al., *Spec. Pap. Geol. Soc. Am.*, *369*, 79–93.

Royer, D. L. (2006), CO_2-forced climate thresholds during the Phanerozoic, *Geochim. Cosmochim. Acta*, *70*, 5665–5675, doi:10.1016/j.gca.2005.11.031.

Royer, D. L., et al. (2001), Paleobotanical evidence for near present-day levels of atmospheric CO_2 during part of the tertiary, *Science*, *292*, 2310–2313, doi:10.1126/science.292.5525.2310.

Samworth, R., and H. Poore (2005), Understanding past ocean circulations: A nonparametric regression case study, *Stat. Model.*, *5*, 289–307, doi:10.1191/1471082X05st102oa.

Sarmiento, J. L., and J. R. Toggweiler (1984), A new model for the role of the oceans in determining atmospheric PCO_2, *Nature*, *308*, 621–624, doi:10.1038/308621a0.

Shackleton, N. J., et al. (1995), Pliocene stable isotope stratigraphy of site 846, *Proc. Ocean Drill. Program Sci. Results*, *138*, 337–355.

Siegenthaler, U., and T. Wenk (1984), Rapid atmospheric CO_2 variations and ocean circulation, *Nature*, *308*, 624–626, doi:10.1038/308624a0.

Siegenthaler, U., et al. (2005), Stable carbon cycle-climate relationship during the late Pleistocene, *Science*, *310*, 1313–1317, doi:10.1126/science.1120130.

Sime, N. G. (2006), Calcium isotope variations in marine and terrestrial carbonates over the past 20 Ma, Ph.D. thesis, Univ. of Cambridge, Cambridge, U. K.

Sime, N. G., et al. (2007), Interpreting the Ca isotope record of marine biogenic carbonates, *Geochim. Cosmochim. Acta*, *71*, 3979–3989, doi:10.1016/j.gca.2007.06.009.

Spencer, D., et al. (1982), *GEOSECS Indian Ocean Expedition*, vol. 6, *Sections and Profiles*, Natl. Sci. Found., Washington, D. C.

Spero, H. J., et al. (2003), Multispecies approach to reconstructing eastern equatorial Pacific thermocline hydrography during the past 360 kyr, *Paleoceanography*, *18*(1), 1022, doi:10.1029/2002PA000814.

Takahashi, T., et al. (1997), Global air-sea flux of CO_2: An estimate based on measurements of sea-air pCO_2 difference, *Proc. Natl. Acad. Sci. U. S. A.*, *94*, 8292–8299, doi:10.1073/pnas.94.16.8292.

Thunell, R. C., and B. H. Corliss (1986), Late Eocene-Early Oligocene carbonate sedimentation in the deep sea, in *Terminal Eocene Events*, edited by C. Pomerol and I. Premoli-Silva, pp. 363–380, Elsevier, Amsterdam.

Turchyn, A. V., and D. P. Schrag (2004), Oxygen isotope constraints on the sulfur cycle over the past 10 million years, *Science*, *303*, 2004–2007, doi:10.1126/science.1092296.

Tyrrell, T., and R. E. Zeebe (2004), History of carbonate ion concentration over the last 100 million years, *Geochim. Cosmochim. Acta*, *68*, 3521–3530, doi:10.1016/j.gca.2004.02.018.

Wanninkhof, R. (1992), Relationship between wind-speed and gas-exchange over the ocean, *J. Geophys. Res.*, *97*, 7373–7382, doi:10.1029/92JC00188.

Wara, M. W., et al. (2005), Permanent El Nino–like conditions during the Pliocene warm period, *Science*, *309*, 758–761, doi:10.1126/science.1112596.

Whitman, J. M., and W. H. Berger (1993), Pliocene-Pleistocene carbon isotope record, site 586, Ontong Java Plateau, *Proc. Ocean Drill. Program Sci. Results*, *130*, 333–348.

Wilkinson, B. H., and T. J. Algeo (1989), Sedimentary carbonate record of calcium and magnesium cycling, *Am. J. Sci.*, *289*, 1158–1194.

Xia, Y. C. (1998), Bias-corrected confidence bands in nonparametric regression, *J. R. Stat. Soc., Ser. B*, *60*, 797–811, doi:10.1111/1467-9868.00155.

Yu, J. M., et al. (2007), B/Ca in planktonic foraminifera as a proxy for surface seawater pH, *Paleoceanography*, *22*, PA2202, doi:10.1029/2006PA001347.

Zachos, J., et al. (2001), Trends, rhythms, and aberrations in global climate 65 Ma to present, *Science*, *292*, 686–693, doi:10.1126/science.1059412.

Zeebe, R. E., and D. A. Wolf-Gladrow (2001), *CO_2 in Seawater: Equilibrium, Kinetics, Isotopes*, Elsevier, Amsterdam.

Zimmermann, H. (2000), Tertiary seawater chemistry: Implications from primary fluid inclusions in marine halite, *Am. J. Sci.*, *300*, 723–767, doi:10.2475/ajs.300.10.723.

C. D. Roberts and A. K. Tripati, Department of Earth Sciences, University of Cambridge, Cambridge CB2 3EQ, UK. (cdr30@esc.cam.ac.uk; atri02@esc.cam.ac.uk)